PCCP

COMMUNICATION

View Article Online
View Journal | View Issue

Cite this: *Phys. Chem. Chem. Phys.*, 2015, **17**, 17584

Received 3rd February 2015,
Accepted 16th June 2015

DOI: 10.1039/c5cp00700c

www.rsc.org/pccp

Nature of the interaction between rare gas atoms and transition metal doped silicon clusters: the role of shielding effects†

Vu Thi Ngan,*[a] Ewald Janssens,[b] Pieterjan Claes,[b] André Fielicke,[c] Minh Tho Nguyen[d] and Peter Lievens*[b]

Mass spectrometry experiments show an exceptionally weak bonding between Si_7Mn^+ and rare gas atoms as compared to other exohedrally transition metal (TM) doped silicon clusters and other Si_nMn^+ (n = 5–10) sizes. The Si_7Mn^+ cluster does not form Ar complexes and the observed fraction of Xe complexes is low. The interaction of two cluster series, Si_nMn^+ (n = 6–10) and Si_7TM^+ (TM = Cr, Mn, Cu, and Zn), with Ar and Xe is investigated by density functional theory calculations. The cluster–rare gas binding is for all clusters, except Si_7Mn^+ and Si_7Zn^+, predominantly driven by short-range interaction between the TM dopant and the rare gas atoms. A high s-character electron density on the metal atoms in Si_7Mn^+ and Si_7Zn^+ shields the polarization toward the rare gas atoms and thereby hinders formation of short-range complexes. Overall, both Ar and Xe complexes are similar except that the larger polarizability of Xe leads to larger binding energies.

Atomic clusters emerge as interesting materials in the size regime between single atoms and nanoparticles, whose properties are strongly influenced by confinement effects. Understanding of their size and composition dependent structures and properties is primordial for further usage. The interactions between clusters and rare gas (RG) atoms are of crucial importance in many experimental techniques. For example, RG complexes are used for action spectroscopy in cluster science due to the inherent weak interaction,[1] Ar titration and tagging have been used to obtain isomer-specific photoelectron spectra for 2D and 3D gold clusters[2,3] and isomer selective infrared (IR) spectra of niobium clusters.[4] In most experimental studies, it has been assumed that the RG atoms do not significantly influence the intrinsic structure and properties of the bare clusters, and are therefore called messenger or spectator atoms. A negligible influence of the RG atoms is inferred from their low adsorption energies and from insignificant differences in measured IR spectra of elemental clusters and their Ar-complexes, such as for V_n^+,[5] Nb_n^+,[6] Ta_n^+ (n = 6–20),[7] Si_n^+ (n = 6–21),[8] as well as for binary Si_nV^+ and Si_nCu^+ (n = 6–11) clusters.[9] Nevertheless, such an assumption is not always applicable. Stronger cluster–RG interactions, which cause discernible changes in the IR spectra of the bare clusters, were observed for some Co_n^+, Au_n, and doped Au_nY clusters.[10–12] Moreover, the RG tagging of some oxide clusters changes the energetic ordering of the isomers, in which case a low-energetic structural isomer, and thus not the ground state structure of the bare cluster, is probed in the experiment.[13] A simple electrostatic picture was put forward to explain the stronger influence of the RG atom, analogous to models often used to interpret the interaction of RG atoms with metal surfaces[14] or metal complexes.[15]

Much effort has been devoted to reveal the nature of interaction between RG and metal surfaces[12,16] or metal-atom complexes.[14,17] There are also a lot of experimental and theoretical results for transition metal cations interacting with RG atoms.[18] However, only a few studies have been reported on RG interaction with clusters. In this communication, we demonstrate that the interaction of cationic transition metal (TM) doped silicon clusters with rare gas atoms is predominantly driven by short-range forces, while the long-range forces become dominant in some cases where the s-electron density on the TM atom along the principal axis hinders the formation of short-range RG complexes due to its shielding effect.

Experimental methods

Mass spectrometric experiments are performed in a molecular beam setup, which contains a dual target-dual laser vaporization

[a] *Department of Chemistry, Quy Nhon University, Quy Nhon, Vietnam. E-mail: vuthingan@qnu.edu.vn*
[b] *Laboratory of Solid State Physics and Magnetism, KU Leuven, B-3001 Leuven, Belgium. E-mail: peter.lievens@fys.kuleuven.be*
[c] *Institute for Optics and Atomic Physics, Technische Universität Berlin, Berlin, Germany*
[d] *Department of Chemistry, KU Leuven, B-3001 Leuven, Belgium*

† Electronic supplementary information (ESI) available: Tables and figures providing more detailed information, divided into four parts: analysis of the mass spectra, dependence of the cluster–RG binding energy on the used functionals, interaction of Si_nMn^+ (n = 6–10) with rare gas atoms (Ar, Xe) and interaction of Si_7TM^+ (TM = Cr, Mn, Cu and Zn) with rare gas atoms (Ar, Xe). See DOI: 10.1039/c5cp00700c

cluster source[19] and a time-of-flight mass spectrometer. Two independent Nd:YAG lasers vaporize the target materials and create a plasma. Subsequent injection of a short pulse of helium cools the plasma and leads to condensation in the clustering channel. This condensation room is followed by a thermalization room, which is thermally isolated from the main body of the source and cooled by a continuous flow of liquid nitrogen. The source parameters are optimized for the formation of cold singly transition metal atom doped silicon clusters. A temperature controller allows for stabilization to any temperature in the 80–320 K range. The formation of cluster–argon and cluster–xenon complexes is induced by addition of a fraction of Ar or enriched ^{129}Xe to the He carrier gas, respectively. After expansion into vacuum the cluster distribution in the molecular beam is analyzed using a reflectron time-of-flight mass spectrometer.[20]

Computational methods

The clusters and their complexes are investigated computationally using density functional theory (DFT). The hybrid B3P86 functional is chosen because its good performance for transition metal doped silicon clusters was proven in the previous studies in which computed vibrational spectra were compared with experimental infrared multiphoton dissociation (IR-MPD) spectra.[9,21] A comparison of other functionals including the M06 functional,[22] which is well known to be suitable for weakly bound systems, has been already made in the previous study on the structure determination of Si_nMn^+.[21] M06 calculations give similar energetics to B3P86, but still do not describe the system that well, even when including the RG ligands, at least in terms of the vibrational spectra. In the present study, the RG–cluster binding energies are also calculated using the two functionals (B3P86, M06) (*cf.* Table S1, ESI†). In general, the M06 gives energetically the same picture as B3P86, but consistently ~0.1 eV higher RG binding energies. Therefore, our discussion hereafter is only based on the B3P86 calculations.

The 6-311+G(d) basis set is applied for the silicon and transition metal atoms. The aug-cc-pVDZ-PP basis set, which explicitly treats up to 26 outer electrons, is used for the Xe atom and includes scalar relativistic effects that are important in predicting the binding energies between metal ions and rare gas atoms.[23] All calculations are performed using the Gaussian 03 package.[24] Natural population analysis is done using the NBO 5.G program. All energies are corrected with zero-point energies (ZPEs) computed at the same level of theory.

Mass spectrometric observations

Typical mass spectra of rare gas complexes of manganese doped cationic silicon, $Si_nMn_m^+$·RG (n = 7–17, m = 0–2, RG = Ar and Xe), are shown in Fig. 1. The upper trace shows manganese doped silicon clusters and their argon complexes measured with the cluster source at 80 K and 1% of Ar in the He carrier gas. The mass spectrum in the lower trace is measured using 0.5% of isotopically enriched xenon (^{129}Xe) in the carrier gas and the source at 120 K. The xenon atom is able to attach to silicon at this temperature and therefore, additionally to $Si_nMn_m^+$·Xe, Xe-complexes are seen for the pure silicon clusters.

The relative intensities of the different species were obtained by fitting the natural isotope distributions of the different species to the measured mass spectra. This way partly overlapping species (because of the isotopic broadening) have been deconvoluted.

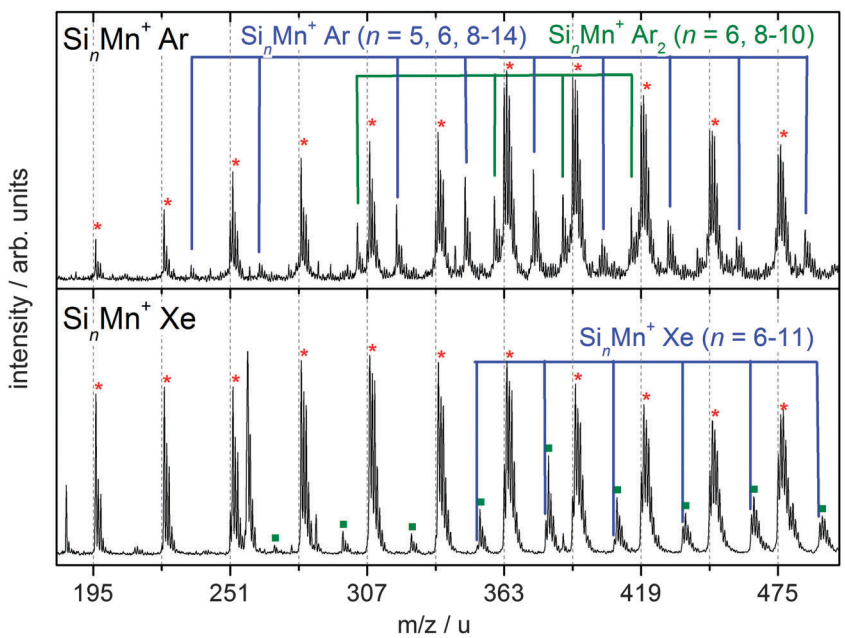

Fig. 1 Mass spectra showing the formation of complexes of Si_nMn^+ with Ar (upper trace) and Xe (lower trace). Bare silicon and Si_n^+–Xe clusters are marked with red stars and green squares, respectively. Manganese doped silicon clusters are represented by the grid lines, doped cluster–RG (RG = Ar, Xe) complexes are indicated by blue lines and cluster–Ar_2 complexes by green lines.

This is required since the atomic mass of Mn is only 1 u less than twice that of the most abundant ^{28}Si isotope and thus significant overlap of the isotopic patterns of pure Si_{n+2}^+, Si_nMn^+, and $Si_{n-2}Mn_2^+$ takes place. As an example the resulting intensities obtained in the measurements using Ar are plotted in Fig. S1 in the ESI† for Si_n^+, Si_nMn^+, $Si_nMn_2^+$, Si_nMn^+·Ar, Si_nMn^+·Ar_2, and $Si_nMn_2^+$·Ar. From this, the cluster size dependent fraction of RG complexes can then be calculated. This fraction is defined as

$$F_{RG} = \frac{I(Si_nMn^+ \cdot RG) + I(Si_nMn^+ \cdot RG_2)}{I(Si_nMn^+) + I(Si_nMn^+ \cdot RG) + I(Si_nMn^+ \cdot RG_2)}$$

with $I(Si_nMn^+)$, $I(Si_nMn^+{\cdot}RG)$, and $I(Si_nMn^+{\cdot}RG)$ representing the integrated abundances of the cluster, its RG and RG_2 complexes, respectively. These fractions are plotted in Fig. 2a for $Si_nMn^+{\cdot}RG$ (n = 5–16) for RG = Ar (red squares) and RG = Xe (black dots).

The degree of RG complex formation can provide precious structural information.[2,3,24] It was, for example, previously demonstrated that no Ar-complex formation was possible (at 80 K) on pure cationic silicon clusters or on endohedral TM-doped silicon cations, while Ar does adsorb on cationic exohedrally TM-doped (Ti, V, Cr, Co, or Cu) Si clusters.[25] Because of its higher polarizability, Xe complexes have been observed for both pure Si clusters and endohedral TM-doped Si clusters.[8,26]

The propensity for RG complex formation, as observed in Fig. 2a, is expected to depend on the strength of the bond between the Si_nMn^+ cluster and the RG atom. The reduced complex formation at the critical size of n = 11 is attributed to the encapsulation of the dopant atom from this size onwards, in line with the observations for other dopants (Ti, V, Cr, Co, and Cu).[25] Surprisingly, the propensity of Ar and Xe complex formation for Si_7Mn^+ is exceptionally low, an effect that has not been observed for any of the other TM dopants studied before. In order to understand why the fraction of $Si_7Mn^+{\cdot}RG$ complexes is so much lower than those of other Si_nMn^+ ($n \leq 10$) clusters, we set out a theoretical study of the chemical bonding of Ar and Xe atoms with two series of clusters: Si_nMn^+ (n = 6–10) and Si_7TM^+ (TM = Cr, Mn, Cu, and Zn). The former series allows the size-dependence of the interaction to be studied, while the latter series concentrates on the role of the electron configuration of the dopant atom.

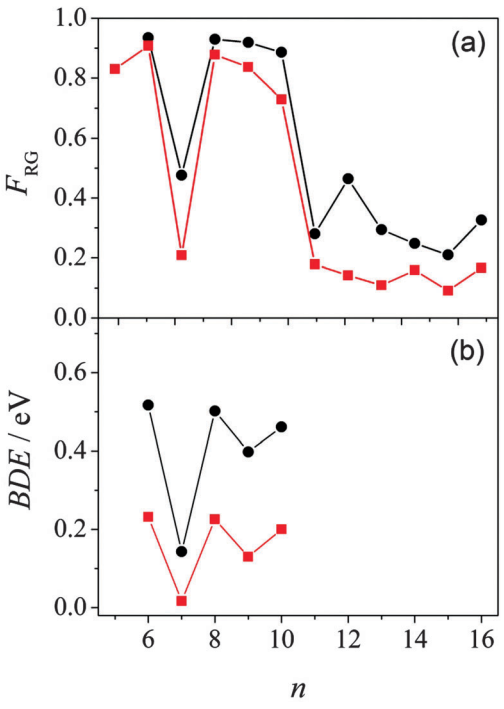

Fig. 2 (a) Cluster size dependent fraction of RG complexes, F_{RG}, for Si_nMn^+ (n = 5–16) for RG = Ar (red squares) and RG = Xe (black dots). (b) Calculated cluster size dependent binding energies between Si_nMn^+ (n = 6–10) and Ar (red squares) or Xe (black dots).

Interaction between Si_nMn^+ (n = 6–10) and Ar, Xe atoms

Structures of Si_nMn^+ clusters were unambiguously identified on the basis of a comparison between measured infrared multiple photon dissociation spectra on the cluster–rare gas complexes and calculated harmonic vibrational counterparts using DFT at the B3P86/6-311+G(d) level.[21] The potential energy surface of the cluster was carefully investigated by searching various structural isomers at different possible spin states. The Si_nMn^+ clusters were concluded to favor the high-spin states such as septet and quintet, while low-spin states (singlet and triplet states) are less stable. These results were later on confirmed by the X-ray magnetic circular dichroism (XMCD) spectroscopy.[27]

In the present study we focus on the cluster–rare gas interaction in the experimentally observed complexes. Structurally, only the exact binding position of the rare gas atom is unsure, as the available IR spectrum was not very sensitive to this. We therefore have searched different isomers of the rare gas complexes and found only two isomers for $Si_7Mn^+{\cdot}RG$ and one stable isomer for other $Si_nMn^+{\cdot}RG$. Due to the weak interaction, the rare gas attachment does not lead to changes in the electronic/spin state of the clusters. The most stable structure of the complexes, consisting of cationic Si_nMn^+ (n = 6–10) and RG = Ar or Xe, are presented in Fig. 3. For $Si_7Mn^+{\cdot}RG$, two stable structural isomers, **Com-A** and **Com-B**, have been identified. The RG directly binds to the Mn dopant atom along an axis connecting the Mn atom with the center of the cluster (principal axis). **Com-B** of $Si_7Mn^+{\cdot}RG$ is an exception in which the RG is bound to the Mn dopant in such a way that the Mn–RG bond is nearly perpendicular to the C_2 axis of Si_7Mn^+.

The Si_nMn^+–RG bond dissociation energy (BDE) is calculated as:

$$BDE(Si_nMn^+{\cdot}RG) = E(Si_nMn^+) + E(RG) - E(Si_nMn^+{\cdot}RG)$$

BDE amounts to ~0.1–0.2 eV for Si_nMn^+·Ar and ~0.4–0.5 eV for Si_nMn^+·Xe with n = 6, 8–10. For Si_7Mn^+ much smaller BDE are found. The stationary structure **Com-A** of Si_7Mn^+·Ar even has negative BDE after correction for ZPEs, meaning that such a complex will only be metastable. **Com-A** of Si_7Mn^+·Xe has an

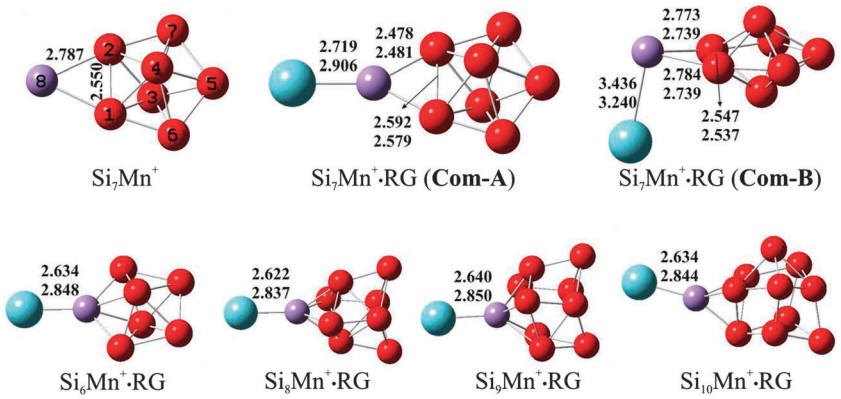

Fig. 3 Structures of Si_nMn^+·RG (n = 6–10, RG = Ar, Xe). Red spheres are Si atoms, purple spheres Mn atoms and blue spheres RG atoms. Selected bond lengths are given in Å, the upper values for the Ar-complexes, and the lower values for the Xe-complexes. The numbering of the atoms of Si_7Mn^+ is applied also for its RG complexes.

exceptionally low BDE of only 0.03 eV. The BDE of **Com-B** is 0.02 eV for Si_7Mn^+·Ar and 0.14 eV for Si_7Mn^+·Xe. Complexes with a BDE larger than ~0.15 eV (such as for Si_nMn^+·RG with n = 6, 8–10 and RG = Ar, Xe) are observed in the mass spectra with higher abundances. Calculations using the M06 functional that also accounts for dispersion interactions give a similar picture, but the interaction energies are consistently ~0.1 eV higher (Table S1, ESI†). These BDE values are consistent with the typical adsorption energies of RG on metal surfaces (being ~0.1–0.2 eV).[28] The lower BDE of **Com-B**, for both RG = Ar and RG = Xe, is in line with the low fraction of RG complexes observed for Si_7Mn^+ (*cf.* Fig. 2a). For the ease of comparison, the dependence of the computed BDE on the cluster size is plotted in Fig. 2b. Qualitatively, this plot reproduces the size dependence of the RG complex formation on cluster size in Fig. 2a. In summary, using DFT calculations, we could reproduce the peculiar behavior of the Si_7Mn^+ toward RG atoms and conclude that the calculated BDE is proportional to F_{RG}.

In an attempt to explain the exceptionally low BDE(RG–Si_7Mn^+) of **Com-A** and **Com-B**, the nature of interaction between Si_nMn^+ and RG atoms is analyzed. For n = 6, 8–10, the Mn–RG distance is calculated to be around 2.6 and 2.8 Å for Ar and Xe, respectively. **Com-A** of Si_7Mn^+ has slightly larger bond lengths of 2.7 and 2.9 Å for Ar and Xe, respectively. Assuming that the nature of interaction in **Com-A** is similar to that of the Si_nMn^+·RG (n = 6, 8–10) complexes, the difference in bond length indicates that the RG interaction with Si_7Mn^+ in **Com-A** is expected to be weaker than that with other cluster sizes. Although **Com-B** of Si_7Mn^+ is energetically more stable than **Com-A**, the Mn–RG distances in **Com-B** are much longer, being 3.44 and 3.24 Å for Ar and Xe, respectively. Noting that both complexes have a septet electronic state as also the bare Si_7Mn^+ cluster, the nature of the cluster–RG interactions in the **Com-A** and **Com-B** must differ significantly from each other.

Four factors usually contribute to the binding energy of complexes: (i) overlap of orbitals from the two interacting fragments (*i.e.*, cluster and RG atom) leading to a polarization and charge transfer; (ii) repulsion between occupied orbitals of the two fragments; (iii) polarization contribution of the RG atom caused by a positive charge at the binding site (*i.e.*, the Mn dopant atom), and (iv) long-range interaction forces caused by higher-order polarization effects and dispersion energy. The last factor is dominant in the case of no orbital overlap. Of these four factors, (ii) induces a decrease in binding energy while the other three tend to increase the bond strength.

Let us now analyze in detail these different contributions to the BDE of the Si_nMn^+·RG (n = 6–10, RG = Ar, Xe, **Com-A** considered for Si_7Mn^+) complexes.

(i) A careful investigation of the valence molecular orbitals (MOs) of the Si_nMn^+ clusters and their RG-complexes points out that the np atomic orbitals (AOs) of the RG atom (3p for Ar and 5p for Xe) strongly overlap with MOs having large contributions of 3d AO (Mn) of Si_nMn^+, causing a charge transfer of ~0.1 e from Ar to Mn, and ~0.2 e from Xe to Mn. However, the orbital overlaps in the complexes of Si_7Mn^+ are weaker, thereby leading to a smaller charge transfer (being only 0.07 and 0.14 e for the Ar- and Xe-complex, respectively). In combination with the earlier discussed size dependence of the Si_nMn^+–RG bond length, it can be concluded that the orbital overlap contribution to the BDE of the Si_nMn^+·RG (n = 6, 8–10) complexes is significant, while it is smaller for Si_7Mn^+·RG. The RG atom is thus less polarized by interaction with MOs of Si_7Mn^+ than by MOs of the other Si_nMn^+ sizes. Natural population analysis of the occupation of Mn orbitals in Si_nMn^+ provides us with two reasons for the special behavior of Si_7Mn^+. Firstly, both the 3d and 4s shells of Mn in Si_7Mn^+ are half-filled ($3d^54s^1$) while in the other cluster sizes there are nearly 6 electrons in the Mn 3d orbitals ($3d^64s^0$). The half-filled Mn 3d shell in Si_7Mn^+ is more stable than the Mn $3d^6$ configuration of the other Si_nMn^+ sizes, leading to a smaller polarization toward AO-np (RG). Secondly, the large electron density of AO-4s (Mn) of Si_7Mn^+ hinders polarization of 3d orbitals (Mn) toward AO of RG. This can be considered as a shielding or screening effect. Similar shielding effects likely also hamper the formation of a bond between the isolated Mn^+ cation ($3d^54s^1$) and Ar.[18] It should be noted, however, while the IR-MPD spectrum for Si_7Mn^+·Xe gives favorable agreement for the calculated spectrum of the isomer shown in Fig. 3 with the $3d^54s^1$ local configuration at the Mn atom,[21] an

independent experimental study finds a magnetic moment at the Mn of only 4 μ_B.[27]

(ii) It is found that the repulsion contribution is negligible in Si_nMn^+·RG complexes for n = 6, 8–10, whereas it is significant for Si_7Mn^+·RG. Indeed, Si_7Mn^+ has two occupied MOs (HOMO and HOMO−5, Fig. 4) having large contributions of AO-4s (Mn). These MOs are characterized by large lobes along the C_2 axis and pointing out the Si_7Mn^+ molecule, which is elucidated by its Mn $3d^54s^1$ electronic configuration. The contribution of AO-4s (Mn) to the MO of Si_7Mn^+ is pictorially emphasized by plots of total and partial density of states shown in Fig. S2 of the ESI.† The HOMO and HOMO−5 of Si_7Mn^+ cause a strong repulsion upon interaction with the occupied AO-*n*p of the RG atom along the C_2 axis. As a result, their energies largely increase in **Com-A** of Si_7Mn^+·Ar leading to a change in the energetic ordering of the MOs relative to those of bare Si_7Mn^+ (*cf.* Fig. 4). In particular, the HOMO of Si_7Mn^+ correlates with the complex's LUMO, and the LUMO of the Si_7Mn^+ with the complex's HOMO. The swap between HOMO and LUMO destabilizes **Com-A**, which is witnessed by its negative BDE. A similar reasoning holds for **Com-A** of Si_7Mn^+·Xe. But the larger polarizability of Xe, which compensates the negative contribution of the repulsion, results in a small positive BDE of 0.03 eV.

(iii) The dipolar polarization significantly contributes to the binding energy as the positive charges on the Mn atoms in Si_nMn^+ are rather large, amounting to ~0.8–1.0 *e*. However, for Si_7Mn^+, the existence of a big lobe of s-character electron density on the C_2 axis prevents the polarization of the charge of Mn toward the RG atoms, due to the shielding effect. In this case, the shielding of the AO-4s (Mn) has a two-fold effect including the less effective nuclear charge (leading to the weaker polarizability by charge) and the less orbital overlap between AO-3d (Mn) and AO-3p (Ar)/5p (Xe).

(iv) The long-range contribution which is caused by higher-order polarization and dispersion is expected to be much smaller than the other three contributions because of the relatively short bond lengths in these complexes.

In summary, the binding energy of the Si_nMn^+·RG (n = 6, 8–10 and RG = Ar, Xe) complexes is mainly determined by the polarization of the RG atoms by the orbital overlap and the large positive charge on Mn. Such bonding mechanism is similar to the familiar explanation for the short-range RG interaction with metal surfaces and metal complexes.[29] The interaction in **Com-A** of Si_7Mn^+ is different. There are two positive and one negative contribution to its BDE. The positive contributions include the polarizations by orbital overlap and by positive charge on Mn, but they are smaller than those of the other cluster sizes due to the screening effect of the AO-4s on the Mn dopant.

We now turn to an understanding of the nature of chemical bonding in **Com-B** of Si_7Mn^+·Ar and Si_7Mn^+·Xe. The different contributions to the BDE of **Com-B** in comparison with **Com-A** are as follows:

(i) Comparing the MOs of **Com-A** and **Com-B** of Si_7Mn^+ we find that the orbital overlap contribution is much smaller in **Com-B** than that in **Com-A**. Indeed, the charge transfer from RG to Mn in **Com-B** is only 0.01 and 0.07 electron for Ar and Xe, respectively, as compared to values of 0.07 and 0.14 electron for **Com-A** with Ar and Xe.

(ii) The repulsion contribution in **Com-B** is much weaker than that in **Com-A**, because the 4s electron density located out of the C_2 axis is smaller than those on the axis. Therefore the ordering of MOs in **Com-B** is similar to that in the Si_7Mn^+ cluster and there is no switch between HOMO and LUMO of Si_7Mn^+ upon formation of **Com-B** (*cf.* Fig. 4).

(iii) Due to the weaker effect of out-of-axis s-electrons, the polarization contribution of the positive charge of Mn towards the RG atom is larger in **Com-B** than in **Com-A**.

(iv) The long-range contribution plays a more important role to the BDE of **Com-B** due to the absence of orbital overlap, which leads to a long distance between Mn and RG atoms.

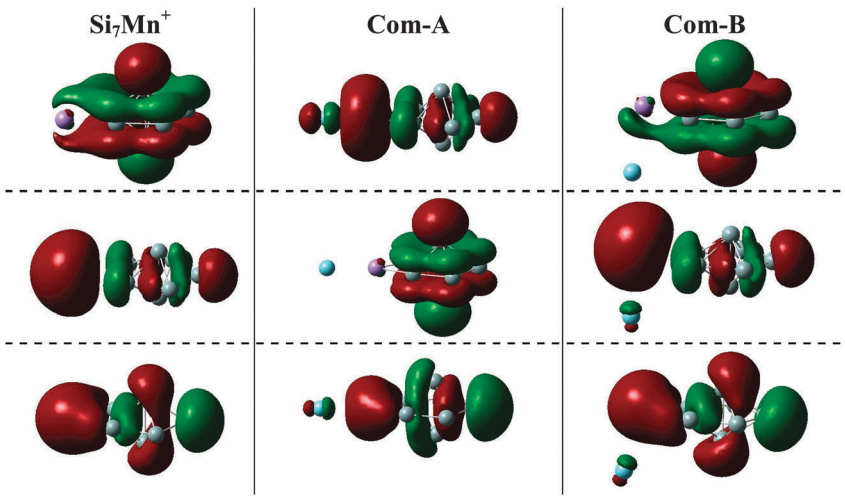

Fig. 4 Selected frontier orbitals of Si_7Mn^+ and **Com-A**, **Com-B** of Si_7Mn^+·Ar. The upper row shows the LUMOs, the middle row the HOMOs, the lower row the HOMO−5 for the bare cluster and **Com-B**, and the HOMO−3 for **Com-A**. Purple spheres are Mn atoms, grey spheres Si atoms and blue spheres Ar atoms.

Moreover, the RG atom in **Com-B** is not only interacting with the Mn but also with the Si atoms (numbered 1, 2, and 3 in Fig. 3).

In summary, for **Com-B** of Si_7Mn^+ the polarization by orbital overlap and repulsion contributes much less to the bonding, whereas the polarization by positive charge and long-range effects including dipole and higher-order polarization bring about the most important parts to the BDE. Due to the main contribution of polarization, the Xe atom possessing higher polarizability interacts stronger with Si_7Mn^+ than the Ar atom, leading to the remarkable observation that the Mn–Xe bond distance (3.24 Å) is shorter than the Mn–Ar distance (3.44 Å) in **Com-B**.

Hence, the nature of the interactions between the RG atoms and Si_nMn^+ (n = 6, 8–10) is predominantly characterized by a polarization of the RG atom due to the orbital overlap and to the positive charge on the Mn dopant. This model for the interaction was used to rationalize the bonding of RG with several pure or doped Si clusters[25] and in the Co_n^+·Ar (n = 4–8) metal cluster complexes.[10] It is also a popular model to explain the interaction of RG atoms with metal surfaces and metal ion complexes.[14,17,29] Avoidance of the symmetrical axis for binding was also found for the Mn^+·(H_2O) complex.[15]

Interaction between Si_7TM^+ with TM = Cr, Mn, Cu, Zn and Ar, Xe atoms

The role of the electronic structure of the dopant atom is unraveled by studying the cluster–RG interaction along the Si_7TM^+ series with TM = Cr, Mn, Cu, and Zn. The clusters are assumed to all have a TM-capped pentagonal bipyramidal structure with C_{2v} symmetry. For Si_7Cr^+, Si_7Mn^+, and Si_7Cu^+ such structures have been identified by combined IRMPD spectroscopy and DFT studies.[9,21,30] No IRMPD data are available to confirm the computed structure for Si_7Zn^+. The clusters have $^6A_1$, $^7A_1$, $^1A_1$, and $^2A_1$ ground electronic states for Si_7Cr^+, Si_7Mn^+, Si_7Cu^+, and Si_7Zn^+, respectively. For each cluster isomer we have investigated different spin states from singlet up to octet and there is little doubt about the ground electronic state of the investigated clusters. The Si_7Cr^+, Si_7Mn^+ favor high-spin states while Si_7Cu^+, and Si_7Zn^+ favor low-spin states, alike the corresponding isolated metal cations. The isolated cations Cr^+ ([Ar]$3d^5 4s^0$) and Mn^+ ([Ar]$3d^5 4s^1$) have half-filled 3d shells, while the Cu^+ ([Ar]$3d^{10} 4s^0$) and Zn^+ ([Ar]$3d^{10} 4s^1$) have totally filled 3d shells. Comparison of the RG interaction with Si_7Zn^+ and Si_7Cu^+ to that with Si_7Mn^+ reveals a stabilizing role of the filled *versus* the half-filled 3d shell in the RG interaction with the TM-capped pentagonal bipyramidal silicon clusters. Comparing the interaction of RG atoms with Si_7Cr^+ to that with Si_7Mn^+ emphasizes the role of the shielding effect of the s-electron in the bonding.

Complex **Com-A** with an Ar atom is only metastable for Si_7Mn^+ while it is stable for Si_7Cu^+ and Si_7Cr^+ with BDEs of 0.22 and 0.19 eV, respectively, even though the Ar–TM bond lengths in Si_7Cu^+·Ar and Si_7Cr^+·Ar (2.46 and 2.82 Å, respectively) are comparable to that in **Com-A** of Si_7Mn^+·Ar. This result means that the nature of interaction of the Ar atoms with Si_7Cu^+ and Si_7Cr^+ is different from that of Ar with Si_7Mn^+. A similar conclusion can be drawn for the corresponding Xe-complexes (*cf.* ESI†).

Similar to Si_7Mn^+, Si_7Zn^+ forms two complexes **Com-A** and **Com-B** with BDE values of −0.40 and 0.01 eV for Ar, and −0.11 and 0.10 eV for Xe, respectively. This indicates that the nature of the RG interaction with Si_7Zn^+ and Si_7Mn^+ is rather similar. However the BDEs of the RG complexes of Si_7Zn^+ are even lower than those of Si_7Mn^+. Experimentally, no adsorption of Ar on Si_nZn^+ clusters is observed.

To investigate further the orbital overlap, the overlap populations (based on the C-squared population analysis, SCPA[31]) between the AOs of Ar and TM dopant atoms in **Com-A** of Si_7TM^+·Ar are plotted in Fig. 5. It can be seen that the orbital overlaps for TM = Cr, Cu are much stronger than for TM = Mn, Zn. The AO-3s (Ar) hardly participate in the overlap, and therefore are not shown in Fig. 5. The AO-3p (Ar) overlap strongly with the AO-3d, 4s, and 4p of TM = Cr or Cu. The AO-3d (TM) overlap less with AO-3p (Ar) in Si_7Mn^+·Ar and the population overlap becomes even zero in the case of Si_7Zn^+·Ar. For the latter, there only is overlap between AO-4p (Zn) and AO-3p (Ar), meaning that the shielding effect of Zn is so strong that the AOs-3d do not participate at all in the overlap, which leads to a polarization.

The valence electronic configuration of the TM atom in the bare cluster Si_7TM^+ computed using NBO analysis are

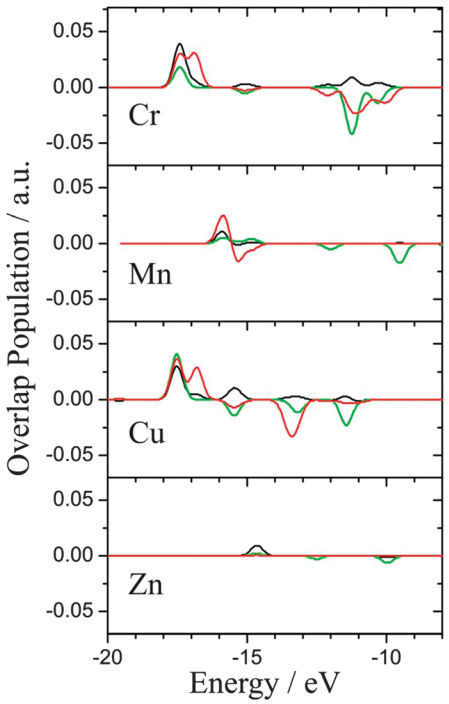

Fig. 5 Overlap population between atomic orbitals of Ar and the TM dopant atoms in **Com-A** of Si_7TM^+ (TM = Cr, Mn, Cu, and Zn). The red curves are overlap populations for 3d(TM)–3p (Ar), green curves for 4s(TM)–3p (Ar), and black curves for 4p(TM)–3p (Ar). The BDEs of the complexes are 0.19, −0.25, 0.22, and −0.40 eV, respectively.

$[3d^{4.9}\ 4s^{0.2}]$, $[3d^{5.1}\ 4s^{1.0}]$, $[3d^{9.9}\ 4s^{0.3}]$, and $[3d^{10.0}\ 4s^{1.2}]$ for TM = Cr, Mn, Cu, and Zn, respectively. Both Cr and Mn thus maintain their half-filled $3d^5$ shell, while both Cu and Zn atoms have a filled $3d^{10}$ shell in the Si_7TM^+ clusters. The electron populations of the Mn and Zn 4s orbitals in the Si_7TM^+ clusters are much larger than those of Cr and Cu. Therefore, the weak orbital overlap of Si_7Mn^+ and Si_7Zn^+ is not related to the stability of half-filled or filled 3d shells of the TM atom, but rather to shielding effects of their 4s electrons.

Regarding the shapes of the frontier MOs (Table S6 of the ESI†), the Si_7TM^+ (TM = Cr, Mn, Cu, and Zn) clusters have similar LUMOs. The Si_7Mn^+ and Si_7Zn^+ clusters have a similar HOMO with a large s-lobe along the C_2 axis whereas Si_7Cr^+ and Si_7Cu^+ have a HOMO with a nodal plane containing the C_2 axis. The MOs with a large s-character on the C_2 axis are unoccupied in the latter. Swaps of HOMO and LUMO, relative to the bare clusters, are found for Si_7Mn^+ and Si_7Zn^+ when forming **Com-A** but not for **Com-B**.

In all cases, the Xe-complexes are similar to the Ar-complexes, except that the polarizability of Xe is larger than that of Ar, leading to larger polarization energies and thus larger BDEs of the Xe-complexes.

Conclusions

In conclusion, the nature of the interactions of RG atoms with most of the investigated exohedral transition metal doped silicon cluster cations (Si_nMn^+ with n = 6, 8–10 and Si_7TM^+ with TM = Cr, Cu) are predominantly characterized by a polarization of the RG atom due to the orbital overlap and the positive charge of the clusters. Both Ar and Xe atoms can form similar complexes, but the interaction of the dopant atoms with Xe is stronger due to a larger polarizability related to the larger size of the Xe atom. Si_7Mn^+ and Si_7Zn^+ appear to be special cases. The RG atom tends to avoid binding with the Mn and Zn dopants on the C_2 axis to form **Com-A** due to a shielding effect of the dopant s-electron density. Formation of $Si_7TM^+{\cdot}RG$ complexes having the **Com-B** shape is essentially characterized by long-range interaction forces.

The findings of the present study can be generalized as follows: clusters having high electron density of s-character toward the principal axis of the molecule are expected to be prevented from complexing by a polarization of the RG atom and a repulsion with the occupied orbitals of the RG atoms, overall leading to a weaker interaction energy in the resulting RG-complexes, and thereby limiting the formation of the latter.

Acknowledgements

This work is supported by the Flemish Fund for Scientific Research (FWO-Vlaanderen), the KU Leuven Research Council (GOA 14/007) and the Deutsche Forschungsgemeinschaft within FOR 1282 (FI 893/4). VTN thanks the Vietnam National Foundation for Science and Technology Development (NAFOSTED) under grant 104.06-2013.06.

References

1 W. H. Robertson and M. A. Johnson, *Annu. Rev. Phys. Chem.*, 2003, **54**, 173–213.
2 W. Huang and L.-S. Wang, *Phys. Rev. Lett.*, 2009, **102**, 153401.
3 S. Gilb, K. Jacobsen, D. Schooss, F. Furche, R. Ahlrichs and M. M. Kappes, *J. Chem. Phys.*, 2004, **121**, 4619–4627.
4 A. Fielicke, C. Ratsch, G. von Helden and G. Meijer, *J. Chem. Phys.*, 2005, **122**, 091105.
5 C. Ratsch, A. Fielicke, A. Kirilyuk, J. Behler, G. von Helden, G. Meijer and M. Scheffler, *J. Chem. Phys.*, 2005, **122**, 124302.
6 (*a*) A. Fielicke, C. Ratsch, G. von Helden and G. Meijer, *J. Chem. Phys.*, 2007, **127**, 234306; (*b*) P. V. Nhat, V. T. Ngan and M. T. Nguyen, *J. Phys. Chem. C*, 2010, **114**, 13210–13218.
7 P. Gruene, A. Fielicke and G. Meijer, *J. Chem. Phys.*, 2007, **127**, 234307.
8 J. T. Lyon, P. Gruene, A. Fielicke, G. Meijer, E. Janssens, P. Claes and P. Lievens, *J. Am. Chem. Soc.*, 2009, **131**, 1115–1121.
9 V. T. Ngan, P. Gruene, P. Claes, E. Janssens, A. Fielicke, M. T. Nguyen and P. Lievens, *J. Am. Chem. Soc.*, 2010, **132**, 15589–15602.
10 R. Gehrke, P. Gruene, A. Fielicke, G. Meijer and K. Reuter, *J. Chem. Phys.*, 2009, **130**, 034306.
11 P. Gruene, D. M. Rayner, B. Redlich, A. F. G. van der Meer, J. T. Lyon, G. Meijer and A. Fielicke, *Science*, 2008, **321**, 674–676.
12 L. Lin, P. Claes, P. Gruene, G. Meijer, A. Fielicke, M. T. Nguyen and P. Lievens, *ChemPhysChem*, 2010, **11**, 1932–1943.
13 (*a*) K. R. Asmis, T. Wende, M. Brummer, O. Gause, G. Santambrogio, E. C. Stanca-Kaposta, J. Dobler, A. Niedziela and J. Sauer, *Phys. Chem. Chem. Phys.*, 2012, **14**, 9377–9388; (*b*) C. Kerpal, D. J. Harding, A. C. Hermes, G. Meijer, S. R. Mackenzie and A. Fielicke, *J. Phys. Chem. A*, 2012, **117**, 1233–1239.
14 J. L. F. Da Silva, C. Stampfl and M. Scheffler, *Phys. Rev. B: Condens. Matter Mater. Phys.*, 2005, **72**, 075424.
15 P. D. Carnegie, B. Bandyopadhyay and M. A. Duncan, *J. Phys. Chem. A*, 2011, **115**, 7602–7609.
16 J. E. Muller, *Appl. Phys. A: Mater. Sci. Process.*, 2007, **87**, 433–434.
17 P. D. Carnegie, B. Bandyopadhyay and M. A. Duncan, *J. Phys. Chem. A*, 2008, **112**, 6237–6243.
18 K. Hirsch, V. Zamudio-Bayer, F. Ameseder, A. Langenberg, J. Rittmann, M. Vogel, T. Möller, B. v. Issendorff and J. T. Lau, *Phys. Rev. A: At., Mol., Opt. Phys.*, 2012, **85**, 062501.
19 W. Bouwen, P. Thoen, F. Vanhoutte, S. Bouckaert, F. Despa, H. Weidele, R. E. Silverans and P. Lievens, *Rev. Sci. Instrum.*, 2000, **71**, 54–58.
20 A. Fielicke, G. von Helden and G. Meijer, *Eur. Phys. J. D*, 2005, **34**, 83–88.
21 V. T. Ngan, E. Janssens, P. Claes, J. T. Lyon, A. Fielicke, M. T. Nguyen and P. Lievens, *Chem. – Eur. J.*, 2012, **18**, 15788–15793.
22 Y. Zhao and D. Truhlar, *Theor. Chem. Acc.*, 2008, **120**, 215–241.
23 P. Pyykko, *J. Am. Chem. Soc.*, 1995, **117**, 2067–2070.

24 M. J. Frisch, *et al.*, *Gaussian 03*, Gaussian, Inc., Wallingford, CT, 2004.
25 E. Janssens, P. Gruene, G. Meijer, L. Woste, P. Lievens and A. Fielicke, *Phys. Rev. Lett.*, 2007, **99**, 063401.
26 P. Claes, E. Janssens, V. T. Ngan, P. Gruene, J. T. Lyon, D. J. Harding, A. Fielicke, M. T. Nguyen and P. Lievens, *Phys. Rev. Lett.*, 2011, **107**, 173401.
27 V. Zamudio-Bayer, L. Leppert, K. Hirsch, A. Langenberg, J. Rittmann, M. Kossick, M. Vogel, R. Richter, A. Terasaki, T. Möller, B. v. Issendorff, S. Kümmel and J. T. Lau, *Phys. Rev. B: Condens. Matter Mater. Phys.*, 2013, **88**, 115425.
28 L. W. Bruch, M. W. Cole and E. Zaremba, *Physical Adsorption: Forces and Phenomena*, Clarendon, Oxford, 1997, p. 229.
29 P. D. Carnegie, B. Bandyopadhyay and M. A. Duncan, *J. Chem. Phys.*, 2011, **134**, 014302.
30 P. Claes, Doctoral thesis, University of Leuven, 2012.
31 P. Ros and G. C. A. Schuit, *Theor. Chim. Acta*, 1966, **4**, 1–12.